Extending the Explanatory Power of Live Cell Imaging by computationally modelling the Execution of Apoptotic Cell Death

H. Huber[1,2], **G. Gomez Estrada**[1], **H. Dussmann**[1], **C. O'Connor**[1], and **M. Rehm**[1,*]

[1]Systems Biology Group, Department of Physiology and Medical Physics, Royal College of Surgeons in Ireland, York Street, Dublin 2, Ireland
[2]Siemens Medical Division, Siemens Ireland, Leeson Close, Dublin 2, Ireland

Intracellular apoptotic signalling networks comprise dozens of simultaneous variables, amongst them protein concentrations, trafficking rates, and transmembrane potentials. Decades of biochemical research identified, isolated and precisely characterized many protein components of these networks. To understand their biological function, quantitative live cell microscopy provides researchers with physiologically highly relevant data on intracellular signalling dynamics in time and space. However, only a limited number of cellular parameters can be detected in parallel. To overcome these limitations and to analyse apoptosis execution on a systems level, we fed both biochemical and imaging data into a computational model of apoptosis execution that quantitatively predicts experimental cellular responses. Here we demonstrate the main principles of this systems approach and describe how it can significantly extend the explanatory power of multi-parametric live cell imaging studies.

Keywords Live cell imaging; GFP; FRET; systems biology; apoptosis

1. Introduction

Live cell imaging is a versatile method to obtain physiologically relevant data on the true spatiotemporal dynamics of cellular signaling processes. However, live cell imaging is restricted in the number of parameters that can be observed in parallel in any single experiment. Mathematical modeling of signaling networks on the other hand offers to monitor all parameters involved in a modeled network synchronously. Even though models are usually based on biochemical data on the individual network components, such simulations are purely theoretical tools and often offer little or no direct comparability to experimental data.

Both live cell imaging as well as mathematical modeling generate quantitative data. In this article we describe how creating compatibility of the input and output parameters of imaging and modeling procedures allows combining both techniques to a powerful new approach that can be employed to predict, validate and understand cellular behavior on a systems level.

1.1 Versatility and Limitations of Live Cell Imaging

The imaging of living cells using advanced epi-fluorescence and confocal microscopy has emerged as a highly successful approach to gain insight into intracellular signaling dynamics in real time and space. The strength of live cell imaging becomes particularly present if cells respond asynchronously after stimulation (individual cellular response) or signaling processes are rapid and/or transient. In comparison, classical biochemical bulk analyses only yield responses averaged from a whole cell population.

The dynamics of many physiological parameters can be visualized by microscopy as a wide range of synthetic and relatively non-toxic dyes are available to measure e.g. intracellular ion concentrations, pH,

* Corresponding author: e-mail: mrehm@rcsi.ie

or transmembrane potentials with high specificity [1, 2]. Selectively labeling proteins of interest became feasible with the discovery and molecular cloning of green fluorescent protein (GFP) and revolutionized cellular and molecular research [3, 4]. The subsequent genetic engineering of spectrally blue and red shifted variants of GFP and other fluorescent proteins allowed the spatiotemporal detection of multiple tagged proteins in parallel in single living cells [5, 6]. Recently, GFP-variants have been generated that can be switched in color by targeted excitation pulses, and now also permit to mark intracellular subpopulations of tagged proteins [7]. Novel approaches covalently labeling proteins of interest with small synthetic dyes allow the use of smaller tags which are less likely to interfere sterically with the functions and interactions of the native proteins [8, 9]. Employing probes with fluorophore pairs spectrally compatible to measure changes in Förster resonance energy transfer (FRET) can deliver valuable data on protein-protein interactions, enzyme activities, or ion concentrations [5, 10-12].

While the available fluorescent probes and techniques provide an unprecedented flexibility in the choice of observable parameters, live cell imaging is limited in the number of channels that can be observed in parallel. Physically restricted by the width of absorption and emission peaks of the common dyes, typically no more than three separate channels can conveniently be observed in parallel. In recent years spectral imaging gained popularity as it allows to extend the number of channels by correcting for the spectral overlap between multiple fluorophores [13, 14].

Apart from these spectral limitations, the achievable temporal resolution and signal to noise ratio is restricted biologically as live cell imaging requires conditions that do not directly harm the living specimen or interfere with its proliferative capacity. Excitation intensity, duration and frequency contribute to the generation of reactive oxygen species and the phototoxic damage of key cellular components such as lipids, nucleic acids or proteins [15, 16]. Approaches aiming to minimize phototoxicity arising from fluorophore excitation therefore are currently being developed [17, 18].

Considering that intracellular signaling networks, even when reduced to only their most important reactions, would require monitoring dozens of processes such as protein-protein interactions, enzymatic activities, or protein localizations in parallel, live cell imaging alone is not sufficient to comprehensively examine intracellular signaling networks.

1.2 Computational Modeling of Intracellular Signaling Networks

A possibility to tackle the complexity of cellular signaling networks is to employ *in silico* models that calculate the dynamics of multiple parallel variables, like temporal concentration profiles of proteins and protein complexes [19]. However, the quality and relevance of computational analyses of biological systems are crucially dependent on their biological integrity and the data available to describe the individual model components. Considerable amounts of quantitative data like intracellular protein concentrations, binding and inhibitory constants, or enzymatic activities are already published in scientific fields that attract the attention of a wide community of scientists. In cancer and apoptosis research for example, decades of biochemical work identified, isolated and precisely characterized many key proteins and reactions involved in the central signaling networks. This knowledge already facilitated several studies that mathematically analyzed elements of apoptotic signaling networks on the systems level [20-24].

A first approach typically is trying to computationally re-model the experimental cellular behaviour. This already may allow to qualitatively understand which signaling modules (e.g. positive and negative feed-back loops) are required to generate the experimentally observed responses (e.g. switch-like cellular decisions or oscillations) [25]. Network remodeling also can help identify those biological parameters that significantly influence or control the cellular responses investigated.

Highly attractive to experimental scientists are computational models that allow the one-to-one comparison of mathematical model predictions to an experimentally measurable signal (Fig.1). Such predictive models can directly assist in generating novel and quantitatively testable research hypotheses [22, 26]. Combining a quantitative experimental technique like live cell microscopy with computational

models thus has the potential to provide an understanding of physiological systems at a comprehensiveness which could not have been achieved with either technique alone.

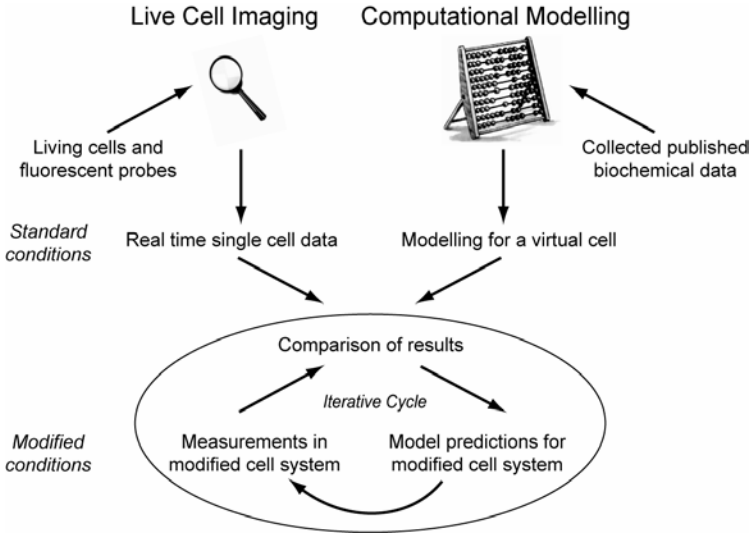

Fig. 1 Schematic workflow for the combination of live cell imaging and computational modeling. Live cell imaging is performed to acquire the real time kinetics of a set of cellular processes. In parallel, a mathematical computer model based on biochemical data of the involved network components is prepared, aiming to re-model the experimental biological responses. Comparison of *in vivo* and *in silico* results allows a first validation of the quality of the generated model. Subsequently, the model can be used to mathematically hypothesize the consequences of modifying biological parameters such as individual protein concentrations. These hypotheses on network behavior and biological consequences then can be investigated experimentally. Experimental findings can in turn refine and/or verify the model, leading to an iterative loop of knowledge generation on systems behavior.

2. Combining Live Cell Imaging and Computational Modelling

Successfully combining imaging and modeling to understand the signaling dynamics of complex networks is dependent on the direct comparability of live cell imaging data and the responses predicted by the computational model. Typically, experimental approaches in cell biology and live cell imaging obey the following sequence:

i) Initially, cells are exposed to a transient or continuous stimulus. The stimulus itself or a subsequent cellular signal triggers a reactions network.

ii) The signaling network translates the input signal into a cellular response. This cellular response is measured either qualitatively or quantitatively.

The computational model needs to be compatible to the experimental approach and thus must fulfill the following prerequisites:

i) The experimental stimulus needs to be represented in the model. If justifiable, the stimulus can be assumed to be present at maximum strength already at the start of the modeling calculation. Otherwise, the stimulus needs to be represented by a dedicated input function.

ii) To allow the direct comparison of the model to the experimental cellular response, the model is required to generate an output resembling the experimental reading.

This fulfilled the combination of live cell imaging and computational modeling can yield novel insights into the underlying regulatory principles and mechanisms controlling signaling networks and their consequences for experimental cellular responses. Using the signaling network of apoptosis execution as an example (Fig.2), in the following we will provide a step-by-step introduction to how multi-parametric imaging can be combined with the benefits of computational modeling.

2.1 Apoptosis Execution and Model Generation

Apoptotic signalling networks represent key signalling matrices in multi-cellular organisms. Apoptotic cell death removes superfluous, damaged and potentially dangerous cells. It is essential during development and indispensable to maintain tissue homeostasis in the adult organism. Disturbed apoptotic signalling can result in enhanced or repressed cell death and may cause degenerative or proliferative diseases. Cell death decisions are believed to be strict and ultimate to ensure the efficient removal of unwanted cells [27, 28].

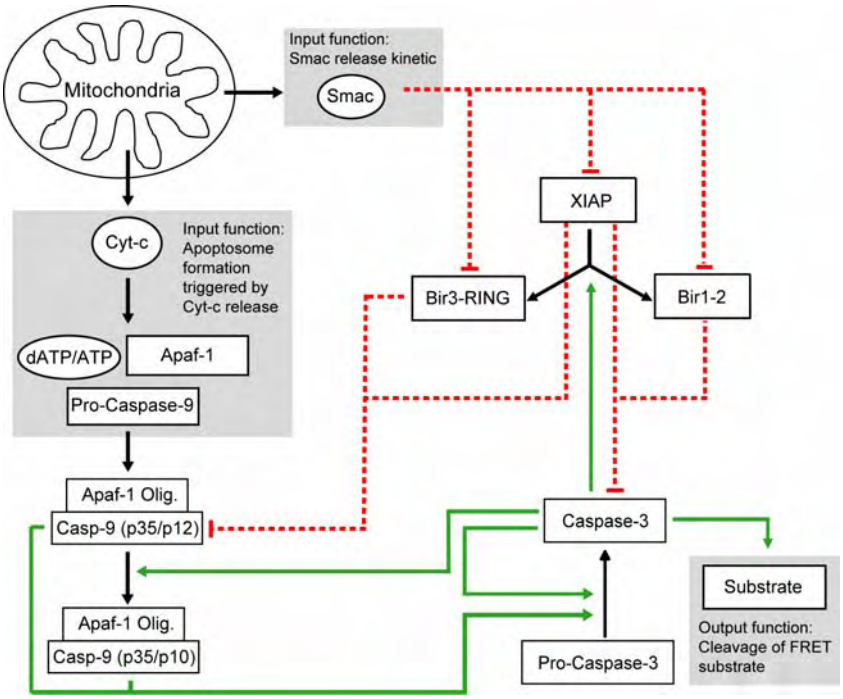

Fig. 2 Simplified schematic representation of the signaling network of apoptosis execution. Enzymatic cleavage processes are shown as green arrows; inhibitory interactions are shown as red dashed lines. Following mitochondrial outer membrane permeabilisation (MOMP), cytochrome-c (Cyt-c) and Smac are concurrently released into the cytosol. Apaf-1 oligomerizes and activates caspase-9 (p35/p12) which in turn can activate executioner caspase-3. Two caspase-3 dependent positive feedbacks ensure a strict cell death response: Caspase-3 cleaves caspase inhibitor XIAP into two fragments (Bir3-RING, Bir1-2) and can process caspase-9 to the (p35/p10)-form which cannot be inhibited by XIAP. XIAP can furthermore be inhibited by Smac. Substrate cleavage by caspase-3 ultimately leads to cell death and can experimentally be measured by a recombinant FRET substrate. Processes in grey boxes serve as input and output functions of the computational model.

2.2 Modelling the initiation of apoptosis execution by input functions

A wide range of different stimuli like death receptor ligands, genotoxic drugs, kinase and proteasome inhibitors, or ionizing radiation have been shown to induce apoptotic cell death. While the signalling pathways induced during the initiation phase of cell death might differ between stimuli, in most cells they converge at the level of mitochondria. At the mitochondria, mitochondrial outer membrane permeabilisation (MOMP) triggers the apoptosis execution network [29]. MOMP has been extensively characterised by live cell imaging approaches and is therefore appropriate to serve as a clearly defined initiating event for the computational model. MOMP results in the synchronous release of intermembrane-space proteins cytochrome-c (cyt-c) and Smac into the cytosol (Fig.2). Their release kinetics can be determined experimentally by live cell microscopy using GFP-fusion variants of cyt-c

and Smac [30, 31] (Fig.3a,b). In an idealized situation, cyt-c and Smac redistribute until a final homogeneous concentration throughout the cell is reached (Fig.3c). In general, such redistributions can mathematically be described by exponential saturation functions *F*:

$$F(t) = C * \left[1 - \exp\left(- \frac{\ln(2)}{t_{1/2}} * t \right) \right] \quad (1)$$

with *C* denoting the saturation concentration and $t_{½}$ the half time of the saturation kinetic. The required protein concentrations can be determined by quantitative biochemistry or taken from the literature if available [22]. Half times can be read directly from experimental traces or determined by mathematical fitting (Fig.3b).

More complex situations might need a different mathematical description of the input. For example, extracellular ligands binding to cell surface receptors, subsequent receptor oligomerisation and adaptor protein recruitment might be driven to a significant extent by cooperative reactions. Reactions with amplifying (positive) or attenuating (negative) cooperativity can be modeled using the Hill equation [32].

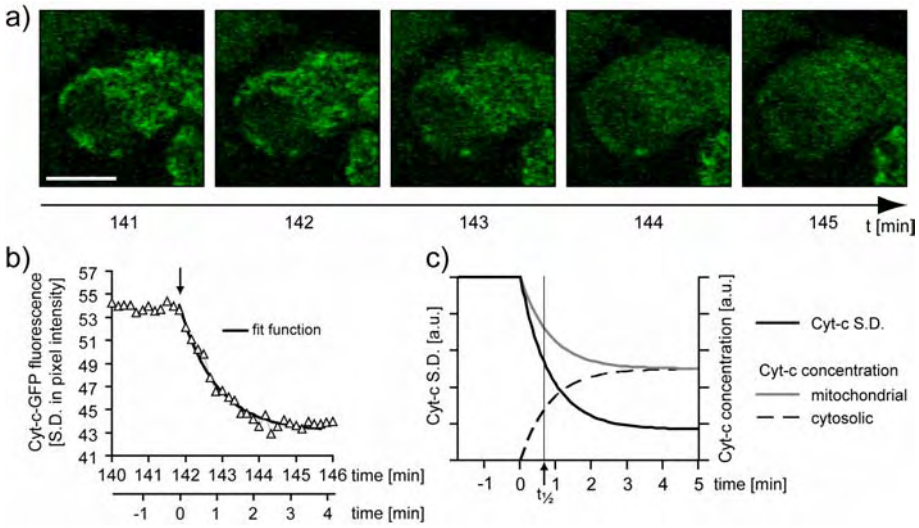

Fig. 3 Generating a saturation input function from imaging data a) Confocal scans show images of a cyt-c-GFP expressing HeLa cell treated with 1 µM staurosporine. Mitochondrial cyt-c-GFP contributes to a high standard deviation of the cellular fluorescence distribution. Upon release, cyt-c homogeneously distributes in the cytosol. Time is displayed in minutes after stimulus addition. Scale bar = 10 µm b) The standard deviation of GFP fluorescence of the cell shown in a) was plotted against time. The onset of release is indicated with an arrow. The release kinetic was fitted with a first order exponential decay function. The second time axis relates time zero to the onset of cyt-c release (MOMP). c) Simplified graphical visualisation of the relationship between intracellular concentration changes and changes in fluorescence S.D. The half-times for S.D. decrease, mitochondrial cyt-c loss and cytosolic cyt-c gain are identical. The increase of cytosolic cyt-c can be modelled with an exponential saturation function.

Computational models need to be carefully balanced between incorporating all necessary reactions and processes and at the same time using a reasonable level of abstraction to avoid unnecessary detail. Abstraction avoids the need to model processes that are poorly understood mechanistically or comprise a set of individual reactions that the modeller is not interested in. Similarly, processes much faster or slower than the modelled time frame might not be required for the simulation. A good example for a justifiable abstraction in the apoptosis execution network is the cyt-c induced formation of the apoptosome (Fig.2). The formation of this large multi-protein complex comprises several complicated reactions requiring cyt-c, Apaf-1, pro-caspase-9 and dATP/ATP and still is not fully understood [33].

Experimentally, apoptosome formation has been shown to be a very rapid process that does not significantly differ from the cyt-c release kinetic itself [30, 34, 35]. Consequently, we may summarize the process of apoptosome formation by equating it with the cyt-c release kinetic:

$$t_{½(\text{Apoptosome})} = t_{½(\text{cyt-c})} \tag{2}$$

Importantly, such simplifications also mean that the model will not be able to yield any predictions on the apoptosome formation process itself. In general, such abstractions in the modeling of any network component are permitted as long as they can be justified.

2.3 Modelling the kinetics of protein interaction networks

In the example of apoptosis execution, the input functions for apoptosome formation and Smac release trigger a subsequent interaction network determined by the interplay of caspase-9, X-linked inhibitor of apoptosis protein (XIAP), Smac, and caspase-3 (Fig.2). This execution network is complex, non-linear, and can proceed in a time frame of minutes [22].

Depending on the biological system and its processes it has to be decided which mathematical approach is most appropriate to simulate the network [36]. The reactions in this as well as in many other protein interaction networks can readily be described by mass-action kinetics represented by a set of coupled ordinary differential equations (ODEs). This approach allows for a unified treatment of diverse biochemical reactions. Modelling the network requires a list of all involved reactions and their respective reaction rates. In the following, we restrict ourselves to comprehensibly illustrating the principles of generating the required ODEs. A more detailed description of a universal mathematical formalism can be found in the literature [37].

2.3.1 Mathematical description of reversible and irreversible reactions

To mathematically model reversible reactions (e.g. binding/dissociation) and irreversible reactions (e.g. enzymatic cleavage reactions or protein modifications that can be assumed to be irreversible), we consider the following exemplary reactions involving the proteins A, B, and C:

$$\begin{aligned} &\text{Binding/dissociation} \quad R_1\text{: A + B} \leftrightarrow \text{AB} \\ &\text{Irreversible cleavage} \quad R_2\text{: C + A} \rightarrow \text{C + A}^{I} + \text{A}^{II}. \end{aligned} \tag{3}$$

Biologically, R_1 for example can reflect protein dimerisations like reversible inhibitor-target interactions. Reaction R_2 can be interpreted as an enzyme C cleaving a substrate A into two fragments A^I and A^{II} without being modified itself.

According to the law of mass action the velocities v_1 and v_2 of reactions R_1 and R_2 are proportional to the product of the concentrations of all reaction partners involved. In the case of reversibility they are additionally balanced between forward and backward reaction:

$$\begin{aligned} v_1 &= k_1^{on} * [A] * [B] \; - k_1^{off} * [AB] \\ v_2 &= k_2^{cleave} * [A] * [C]. \end{aligned} \tag{4}$$

The individual rate constants for binding (k^{on}), dissociation (k^{off}) and cleavage (k^{cleave}) can be taken from the characterisation of these reactions in the published literature or need to be measured experimentally. Based on v_1 and v_2 we can describe the temporal concentration changes for each of the involved protein fractions:

$$\frac{d[A]}{dt} = -v_1 - v_2 = -k_1^{on} * [A] * [B] \; + k_1^{off} * [AB\;] - k_2^{cleave} * [A] * [C]$$

$$\frac{d[B]}{dt} = -v_1 = -k_1^{on} * [A] * [B] \; + k_1^{off} * [AB]$$

$$\frac{d[AB]}{dt} = v_1 = k_1^{on} * [A] * [B] - k_1^{off} * [AB]$$

$$\frac{d[C]}{dt} = 0 \Rightarrow [C] = const. \tag{5}$$

The above constitutes a set of ODEs coupled via the variables [*A*], [*B*], and [*AB*]. We deliberately omitted the reactions describing the cleavage products A^I and A^{II} since these are end products which themselves do not feed back into the reactions. Their temporal behaviour can be obtained independently by $d[A^I]/dt = d[A^{II}]/dt = v_2$.

2.3.2 Remodeling cellular protein concentrations and protein turnover

Besides the above modelled protein interactions, one also needs to consider that the cellular signalling network might be able recover from the signalling processes, leading to the re-establishment of the initial conditions. Living cells implement this by degrading protein products generated by the signalling processes and by replenishing depleted proteins by *de novo* synthesis. Therefore, we will briefly demonstrate how to mathematically describe protein turnover by degradation and synthesis.

To model protein degradation, the degradation velocity *v* of a protein *A* can be expressed as:

$$v^{\deg} = \frac{d[A]}{dt} = -k^{\deg} * [A] \tag{6}$$

with [*A*] denoting the concentration of protein A and k^{deg} its individual degradation rate in [s^{-1}].

For a living cell we assume a steady state protein concentration which is fulfilled by compensating degradation by protein production:

$$\frac{d[A]}{dt} = k^{prod} - k^{\deg} * [A] = 0 \tag{7}$$

with k^{prod} denoting the production rate of protein *A* in [M*s^{-1}].

The cellular concentration (steady state concentration [A_0]) of individual proteins and their respective degradation rates can be measured experimentally by quantitative biochemistry [22, 38]. From these data the protein production rate k^{prod} then calculates as

$$k^{prod} = k^{\deg} * [A_0]. \tag{8}$$

Based on the production and degradation rates the relaxation velocity for any concentration of protein A back towards the steady state concentration [A_0] can be expressed as

$$v_A = k^{prod} - k^{\deg} * [A]. \tag{9}$$

Individual protein turnover kinetics (v_A, v_B, v_C) can then be assigned to the proteins A and B in the example outlined above (Eqs.(3),(5)). As the protein complex AB in the above example is generated by the reaction network itself, a pure degradation term (Eq.(6)) applies for [*AB*]. With the concentration of C being constant in time, we obtain:

$$\frac{d[A]}{dt} = -v_1 - v_2 + v_A \qquad \frac{d[B]}{dt} = -v_1 + v_B$$
$$\frac{d[AB]}{dt} = v_1 + v_{AB} \tag{10}$$

2.3.3 Mathematical solution and graphical presentation of a reaction network

Input functions (Eq.(1)), the above system of nonlinear ODEs (Eq. (10)) and the respective reaction rates and steady state protein concentrations can then be typed into standard software suites like MATLAB (The Mathworks, US) and be numerically solved. The concentration changes of the respective proteins are typically calculated stepwise from one time point to the next using adaptive step Runge-Kutta solvers (Gear74). The temporal protein profiles can be plotted as for example shown for Fig.4 for a selection of proteins fractions during apoptosis execution. Such a model can also form the basis for subsequent mathematical analyses of the stability and robustness of cellular decision matrices [20, 21, 23].

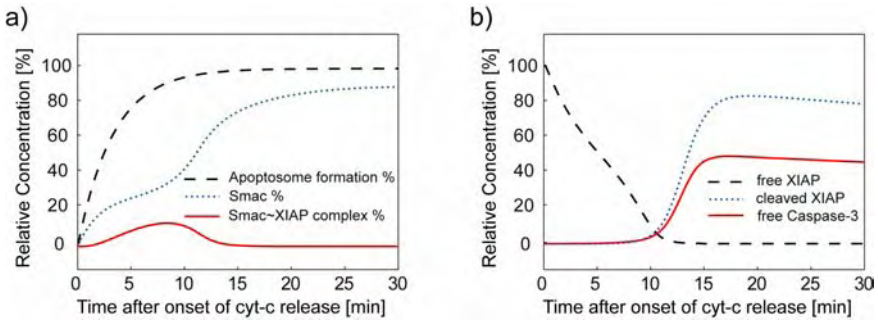

Fig. 4 Calculation and plotting of selected protein profiles during apoptosis execution. a) Apoptosome formation as an input function initiates the network. Smac release from the mitochondria as the second input function is shown as well. The Smac profile however is already affected by the reaction network, as XIAP binds to a fraction of the Smac protein. b) The amount of free XIAP is consumed by Smac-binding. Furthermore, upon caspase-3 activation, XIAP is cleaved and its cleavage products accumulate. Protein profiles were calculated from a set of ODEs modeling apoptosis execution [22].

Other biological systems might require different mathematical approaches. Modelling rapid intracellular signalling processes (seconds or sub-seconds time scale) or processes in large or polarized cells like neurons might require taking spatial concentration gradients into account which arise from diffusion or active transport processes. At conditions of low reactant concentrations in small volumes the limited absolute number of reactant molecules might also require utilizing stochastic models which take the probability of a reaction to occur into account [39].

2.4 Comparison of experimental response and output function

While an ODE-based model can calculate the temporal behaviour of various protein fractions it usually does not automatically calculate an output parameter that can be compared to the experimental signal. Experimental outputs in live cell imaging typically are fluorescence signals which can be related to cellular cellular physiological parameters by calibration procedures. Using intracellular caspase-3 activity during apoptosis execution as an example, in the following section we will demonstrate how to link mathematical model to the experimental signal via a dedicated output function.

Efficient activation of executioner caspase-3 (Fig.2) orchestrates the coordinated apoptotic demise of cells by cleaving a wide range of intracellular substrates [40]. Caspase-3 activity can be monitored microscopically by the cleavage of recombinant FRET substrates (Fig.5a). These substrates are highly specific probes comprised of FRET-compatible GFP variants fused via a caspase-3 specific linker region [41, 42]. Upon cleavage of the FRET substrate, the disruption of resonance energy transfer results in an increased donor (CFP) fluorescence (Fig.5b). FRET probes specific for various cellular parameters have been developed so far and their use becomes increasingly popular, as they allow a noise-reduced ratiometric readout [11, 12].

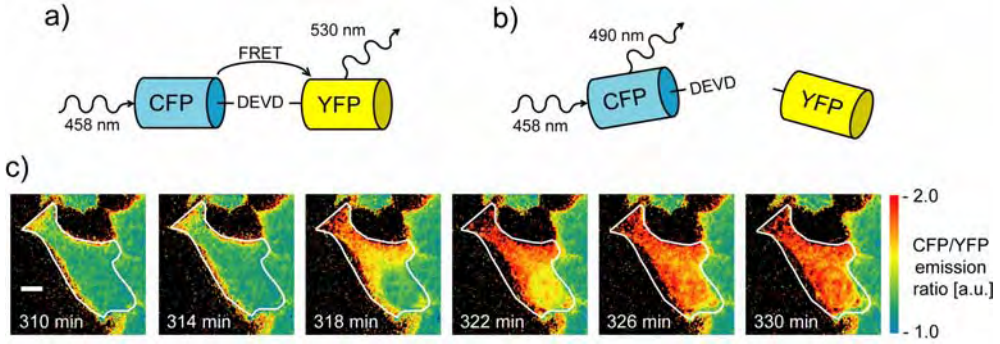

Fig. 5 Detection of caspase-3 activity by cleavage of a recombinant FRET probe. **(a)** In the intact probe upon CFP excitation energy is transferred from donor CFP to acceptor YFP by resonance energy transfer. **(b)** Cleavage of the linker region results in disruption of resonance energy transfer and an increased CFP emission. **(c)** Caspase-3 activation indicated by FRET probe cleavage following MOMP in a single living HeLa cell treated with 1 µM staurosporine [22]. The increase in CFP emission is displayed as a ratio to the YFP emission resulting from direct YFP excitation. Time is displayed in minutes after stimulus addition. Scale bar = 5 µm.

The FRET substrate cleavage by caspase-3 can be modelled by an additional reaction:

$$\textit{Caspase-3} + \textit{Substrate} \rightarrow \textit{Caspase-3} + \textit{Cleaved\_Substrate} \tag{11}$$

Following mass action kinetics, the rate of substrate cleavage is proportional to the concentrations of *Caspase-3* and *Substrate*. Written as an ODE the temporal profile of substrate cleavage can be expressed as follows:

$$\frac{d\left[Substrate\right]}{dt} = -k^{cleave} * [Substrate] * [Caspase-3], \tag{12}$$

with k^{cleave} denoting the rate constant of the reaction. Solving Eq.(12) for *Substrate*, we get

$$[Substrate]\ (t) = [Substrate](0) * \exp\left(-k^{cleave} * \int_0^t [Caspase-3](t)dt\right) . \tag{13}$$

This equation describes the loss of substrate as a cumulative function of temporal caspase-3 activity with [*Substrate*](0) denoting the initial amount of available FRET substrate. The loss in *Substrate* directly corresponds to an increase in *Cleaved_Substrate*:

$$[Cleaved\_Substrate](t) = [Substrate](0) - [Substrate](t) , \tag{14}$$

The increase of *Cleaved_Substrate* over time can be found by substituting Eq.(13) in Eq.(14):

$$[Cleaved\_Substrate](t) = [Substrate](0) * \left[1 - \exp\left(-k^{cleave} * \int_0^t [Caspase-3](t)dt\right)\right] . \tag{15}$$

The ratio of Cleaved_Substrate(t)/Substrate(0) then can directly be compared to the temporal profile of the experimental CFP/YFP emission ratio:

$$\frac{[Cleaved\_Substrate](t)}{[Substrate](0)} = \left[1 - \exp\left(-k^{cleave} * \int_0^t [Caspase-3](t)dt\right)\right] . \tag{16}$$

Adding Eq.(16) as an output function to the ODE equation system we have generated a model comprising input functions, a reaction network and an output suitable for direct comparison with experimental data. Initially, a comparison of model responses to the experimental responses of the modelled cell line will yield information on the quality of the model generated (Fig.1, Fig.6a,b) and might require additional fine tuning. Once the model corresponds to the biological reference system, individual parameters or parameter combinations such as protein concentrations or rate constants can be modified, quantitative predictions be generated and subsequently be validated experimentally. Exemplary comparisons of model predictions and cellular responses upon altering the intracellular concentration of caspase inhibitor XIAP are displayed in Fig.6. It is important to note that these predictions are not universally valid but specific for the cell type modelled. For example while native XIAP expression levels were mathematically and experimentally shown not to significantly inhibit apoptosis execution in HeLa cells, in sympathetic neurons native XIAP expression efficiently inhibits apoptosis execution following MOMP [22, 43]. Modelling thus can also help to highlight and explain that one and the same protein can exert different roles in different cell types.

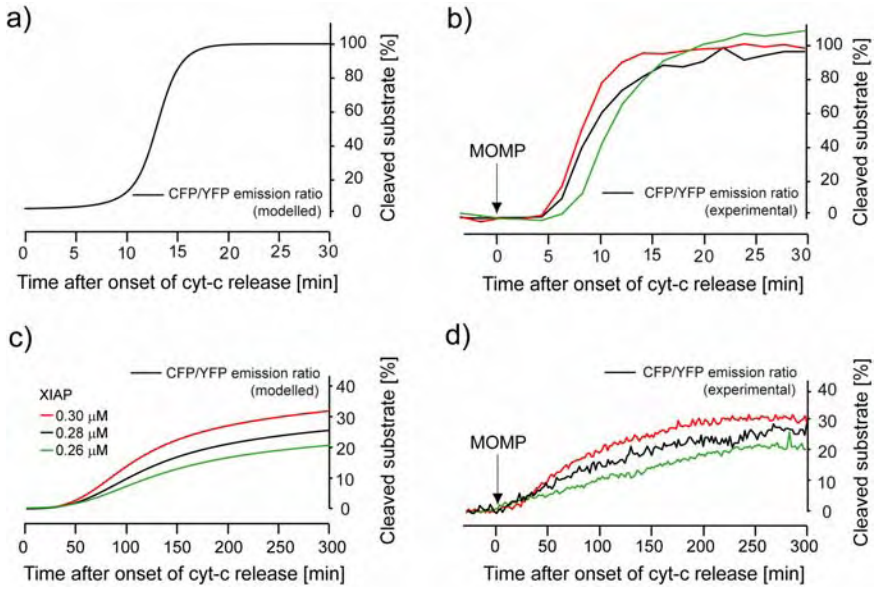

Fig. 6: Comparison of model predictions and experimental responses [22]. **a**) Mathematical predictions for caspase-3 dependent FRET substrate cleavage in a modeled HeLa cell. **b**) Experimental FRET disruption traces for three individual HeLa cells following treatment with 1 µM staurosporine. **c**) Mathematical modeling for caspase-3 dependent FRET substrate cleavage upon overexpression of XIAP in HeLa cells predicts slow and incomplete cleavage of the FRET substrate. **d**) HeLa cells overexpressing XIAP at concentration ranges modeled in c) quantitatively closely resemble the mathematical predictions.

3. Outlook

Employing mathematics to describe, understand and predict processes in nature is indispensable and has a long and impressive history in the fields of physics, chemistry and their respective applied engineering disciplines. While mathematics also play a central role in many fields of biology, remodeling or even predicting cellular signaling by mathematical simulations, especially in genetic and protein interaction networks, is often hampered by the complexity of the systems and the unavailability of the required experimental data and methodology. The progress made in live cell imaging technology in the past decade now offers an appropriate platform for cell biologists that allows the testing of computationally generated research hypotheses. The combination of microscopy and cellular modeling holds great

potential to significantly extend the explanatory power of live cell imaging by allowing a comprehensive understanding of the regulation of cellular signaling.

However, successfully combining both fields is not an easy task. For the practical implementation of systems biology projects, a major concern is the deficit in quantitative biochemical data on intracellular protein concentrations which are required for the generation of cell type specific models. Furthermore, appropriate data archiving and database standards are only now being developed [44]. While research projects in cell biology routinely analyze the consequences of protein overexpression, downregulation or knock out, an absolute quantification of proteins so far was seldom required to answer classical research hypotheses. The need for quantitative biochemistry has dramatically increased with the rapid development of systems biology in recent years. Even if quantitative data are available questions may arise about their reliability and reproducibility. Experimental protocols may differ significantly between laboratories and may cause inconsistencies in the published parameters. For example, documented enzyme activities for caspase-3 for different substrates at different conditions can vary by a factor of 100 [45-48]. It requires an excellent biochemical understanding of the methodology to appropriately interpret the published literature and choose biological meaningful parameters.

Systems biology projects require interdisciplinary teams with expertise in both experimental biology and mathematics, disciplines that share little or no scientific language. Successful implementation therefore also heavily relies on communication skills and open mindedness for the project partner's approaches to the scientific questions. So far, theoretical models for many cellular signaling pathways have been generated and the respective program codes in most cases are freely available. Following the need for standardization, dedicated online repositories have been set up to archive and curate peer-reviewed published models (see for example http://biomodels.net; http://vcell.org). Microscopists daring to explore the possibilities of experimental systems biology may be surprised to find a wealth of theoretical mathematical tools that are available to be modified and linked to their experimental questions.

Acknowledgements Parts of the figures were reproduced from [22] with kind permission from Nature Publishing Group. This work was supported by grants from Science Foundation Ireland (05/RFP/BIM0056) and the Health Research Board (RP/2006/258) awarded to MR.

References

[1] R.P. Haugland, in: Handbook of fluorescent probes and research products, Vol.10. (Molecular Probes Inc., 2005)
[2] W.T. Mason, in: Fluorescent and luminescent probes for biological activity, 2nd edition, Biological techniques series, (Academic press, London, 1999)
[3] D.C. Prasher, V.K. Eckenrode, W.W. Ward, F.G. Prendergast, and M.J. Cormier, Gene, **111**(2): p. 229-33.(1992)
[4] O. Shimomura, F.H. Johnson, and Y. Saiga, J Cell Comp Physiol, **59**: p. 223-39. (1962)
[5] D.M. Chudakov, S. Lukyanov, and K.A. Lukyanov, Trends Biotechnol, **23**(12): p. 605-13. (2005)
[6] R.Y. Tsien, Annu Rev Biochem, **67**: p. 509-44. (1998)
[7] K.A. Lukyanov, D.M. Chudakov, S. Lukyanov, and V.V. Verkhusha, Nat Rev Mol Cell Biol, **6**(11): p. 885-91. (2005)
[8] B.N. Giepmans, S.R. Adams, M.H. Ellisman, and R.Y. Tsien, Science, **312**(5771): p. 217-24. (2006)
[9] T. Gronemeyer, G. Godin, and K. Johnsson, Curr Opin Biotechnol, **16**(4): p. 453-8. (2005)
[10] R.B. Sekar and A. Periasamy, J Cell Biol, **160**(5): p. 629-33. (2003)
[11] I.T. Li, E. Pham, and K. Truong, Biotechnol Lett, **28**(24): p. 1971-82. (2006)
[12] B.A. Pollok and R. Heim, Trends Cell Biol, **9**(2): p. 57-60. (1999)
[13] Y. Garini, I.T. Young, and G. McNamara, Cytometry A, **69**(8): p. 735-47. (2006)
[14] T. Zimmermann, J. Rietdorf, and R. Pepperkok, FEBS Lett, **546**(1): p. 87-92. (2003)
[15] M.M. Knight, S.R. Roberts, D.A. Lee, and D.L. Bader, Am J Physiol Cell Physiol, **284**(4): p. C1083-9. (2003)
[16] R. Dixit and R. Cyr, Plant J, **36**(2): p. 280-90. (2003)
[17] R.A. Hoebe, C.H. Van Oven, T.W. Gadella, Jr., P.B. Dhonukshe, C.J. Van Noorden, and E.M. Manders, Nat Biotechnol, **25**(2): p. 249-53. (2007)
[18] T. Nishigaki, C.D. Wood, K. Shiba, S.A. Baba, and A. Darszon, Biotechniques, **41**(2): p. 191-7. (2006)
[19] B.B. Aldridge, J.M. Burke, D.A. Lauffenburger, and P.K. Sorger, Nat Cell Biol, **8**(11): p. 1195-203. (2006)

[20] M. Bentele, I. Lavrik, M. Ulrich, S. Stosser, D.W. Heermann, H. Kalthoff, P.H. Krammer, and R. Eils, J Cell Biol, **166**(6): p. 839-51. (2004)
[21] T. Eissing, H. Conzelmann, E.D. Gilles, F. Allgower, E. Bullinger, and P. Scheurich, J Biol Chem, **279**(35): p. 36892-7. (2004)
[22] M. Rehm, H.J. Huber, H. Dussmann, and J.H. Prehn, Embo J, **25**(18): p. 4338-49. (2006)
[23] S. Legewie, N. Bluthgen, and H. Herzel, PLoS Comput Biol, **2**(9): p. e120. (2006)
[24] M. Fussenegger, J.E. Bailey, and J. Varner, Nat Biotechnol, **18**(7): p. 768-74. (2000)
[25] B.N. Kholodenko, Nat Rev Mol Cell Biol, **7**(3): p. 165-76. (2006)
[26] N.A. van Riel, Brief Bioinform, **7**(4): p. 364-74. (2006)
[27] S. Holdenrieder and P. Stieber, Clin Biochem, **37**(7): p. 605-17. (2004)
[28] D.E. Bredesen, R.V. Rao, and P. Mehlen, Nature, **443**(7113): p. 796-802. (2006)
[29] D.R. Green and G. Kroemer, Science, **305**(5684): p. 626-9. (2004)
[30] J.C. Goldstein, N.J. Waterhouse, P. Juin, G.I. Evan, and D.R. Green, Nat Cell Biol, **2**(3): p. 156-62. (2000)
[31] M. Rehm, H. Dussmann, and J.H. Prehn, J Cell Biol, **162**(6): p. 1031-43. (2003)
[32] A.V. Hill, J. Physiol. (London). **40**: p. 4-7. (1910)
[33] S.J. Riedl and G.S. Salvesen, Nat Rev Mol Cell Biol, **8**(5): p. 405-13. (2007)
[34] M.M. Hill, C. Adrain, P.J. Duriez, E.M. Creagh, and S.J. Martin, Embo J, **23**(10): p. 2134-45. (2004)
[35] D. Twiddy, D.G. Brown, C. Adrain, R. Jukes, S.J. Martin, G.M. Cohen, M. MacFarlane, and K. Cain, J Biol Chem, **279**(19): p. 19665-82. (2004)
[36] J.J. Tyson, K. Chen, and B. Novak, Nat Rev Mol Cell Biol, **2**(12): p. 908-16. (2001)
[37] O. Wolkenhauer, M. Ullah, P. Wellstead, and K.H. Cho, FEBS Lett, **579**(8): p. 1846-53. (2005)
[38] A. Belle, A. Tanay, L. Bitincka, R. Shamir, and E.K. O'Shea, Proc Natl Acad Sci U S A, **103**(35): p. 13004-9. (2006)
[39] M. Ullah, H. Schmidt, K.H. Cho, and O. Wolkenhauer, Syst Biol (Stevenage), **153**(2): p. 53-60. (2006)
[40] U. Fischer, R.U. Janicke, and K. Schulze-Osthoff, Cell Death Differ, **10**(1): p. 76-100. (2003)
[41] M. Rehm, H. Dussmann, R.U. Janicke, J.M. Tavare, D. Kogel, and J.H. Prehn, J Biol Chem, **277**(27): p. 24506-14. (2002)
[42] L. Tyas, V.A. Brophy, A. Pope, A.J. Rivett, and J.M. Tavare, EMBO Rep, **1**(3): p. 266-70. (2000)
[43] P.R. Potts, S. Singh, M. Knezek, C.B. Thompson, and M. Deshmukh, J Cell Biol, **163**(4): p. 789-99. (2003)
[44] H.J. Huber, M. Rehm, M. Plchut, H. Dussmann, and J.H. Prehn, Bioinformatics, **23**(5): p. 648-50. (2007)
[45] L. Casciola-Rosen, D.W. Nicholson, T. Chong, K.R. Rowan, N.A. Thornberry, D.K. Miller, and A. Rosen, J Exp Med, **183**(5): p. 1957-64. (1996)
[46] M. Garcia-Calvo, E.P. Peterson, B. Leiting, R. Ruel, D.W. Nicholson, and N.A. Thornberry, J Biol Chem, **273**(49): p. 32608-13. (1998)
[47] H.R. Stennicke, J.M. Jurgensmeier, H. Shin, Q. Deveraux, B.B. Wolf, X. Yang, Q. Zhou, H.M. Ellerby, L.M. Ellerby, D. Bredesen, D.R. Green, J.C. Reed, C.J. Froelich, and G.S. Salvesen, J Biol Chem, **273**(42): p. 27084-90. (1998)
[48] H.R. Stennicke, M. Renatus, M. Meldal, and G.S. Salvesen, Biochem J, **350 Pt 2**: p. 563-8. (2000)